(15) Koningsveld, R.; Kleintjens, L. A. *Macromolecules* **1971**, *4*, 637.
(16) Kirkwood, J. G.; Buff, F. P. *J. Chem. Phys.* **1951**, *19*, 774.
(17) Zimm, B. H. *J. Chem. Phys.* **1953**, *21*, 934.
(18) Zimm, B. H.; Lundberg, J. L. *J. Phys. Chem.* **1956**, *60*, 425.
(19) Fixman, M. *J. Chem. Phys.* **1960**, *35*, 889.
(20) Huggins, M. L. *J. Phys. Chem.* **1971**, *75*, 1255.
(21) Renuncio, J. A. R.; Prausnitz, J. M. *Macromolecules* **1969**, *9*, 898.
(22) Brandani, V. *Macromolecules* **1979**, *5*, 883.
(23) Huggins, M. L. *Ann. N. Y. Acad. Sci.* **1942**, *43*, 9.
(24) Miller, A. R. *Proc. Cambridge, Philos. Soc.* **1943**, *39*, 54.
(25) Guggenheim, E. A. *Proc. R. Soc. London, Ser. A.* **1944**, *183*, 203.
(26) Unpublished results, 1987.
(27) Krigbaum, W. R.; Geymer, D. O. *J. Am. Chem. Soc.* **1959**, *81*, 1859.
(28) Saeki, S.; Holste, J. C.; Bonner, D. C. *J. Polym. Sci., Polym. Phys.* **1983**, *21*, 2049.
(29) Eichinger, B. E.; Flory, P. J. *Trans. Faraday Soc.* **1968**, *64*, 2066.
(30) Lundberg, J. L. *J. Macromol. Sci. Phys.* **1969**, *B3*(4), 693.
(31) Flory, P. J.; Daoust, H. *J. Polym. Sci.* **1957**, *25*, 429.
(32) Sanchez, I. C.; Lacombe, R. H. *Macromolecules* **1978**, *11*, 1145.
(33) Hamada, F.; Shiomi, T.; Fugiwara, K.; Nakajima, A. *Macromolecules* **1980**, *13*, 729.
(34) Sanchez, I. C.; Lohse, D. J. *Macromolecules* **1981**, *14*, 131.
(35) Masegosa, R. M.; Prolongo, M. G.; Horta, A. *Macromolecules* **1986**, *19*, 1478.
(36) Nakajima, N.; Huang, C. D. *J. Macromol. Sci. Phys.* **1986**, *B25*(4), 395.
(37) Kuwahara, N.; Okazawa, T.; Kaneko, M. *J. Polym. Sci., Part C* **1968**, *23*, 543.

# Ordered Packing Arrangements of Spherical Micelles of Diblock Copolymers in Two and Three Dimensions

**Edwin L. Thomas,* David J. Kinning,† David B. Alward,‡ and Chris S. Henkee**

*Polymer Science and Engineering Department, University of Massachusetts, Amherst, Massachusetts 01003.* *Received October 29, 1986*

ABSTRACT: Structural data are presented on the ordered arrangements of spherical micelles of diblock copolymers in two dimensions [transmission electron microscopy (TEM) of solution cast films containing a single layer of domains] and in three dimensions [TEM of microtomed sections and small-angle X-ray scattering (SAXS) from bulk samples]. The lattice type of the micelle cores in the two-dimensional thin film is hexagonal, and in the three-dimensional bulk state it is body centered cubic. A simple packing model that addresses the problem of uniform covering of the matrix space by the corona chains for a given lattice suggests that considerable interpenetration of neighboring micelle segmental density profiles occurs. The mode of packing is dictated by the optimal covering lattice that minimizes the unfavorable deformation of the matrix chains as they uniformly fill the matrix space.

## Introduction

There have been numerous studies of the morphology and thermodynamics of block copolymers in the last two decades. The scale of microphase separation is typically hundreds of angstroms so that SAXS and TEM have proven to be useful techniques for structural investigations. Such studies established that under nearly equilibrium conditions, the microphase separation results in the formation of regular arrays of spheres, cylinders or lamellae, depending on the volume fractions of the components.[1] Recently an additional morphology, that of the ordered bicontinuous double diamond structure, was discovered.[2]

Theoretical statistical mechanical treatments of block copolymers have been primarily concerned with the location of the microphase transition and with elucidation of the ranges of the various sample morphologies (e.g., spheres, cylinders, lamellae) as a function of molecular weight and composition. In the compositional range for spherical microdomains (micelles), the treatments of Meier[3] and Helfand and Wasserman[4] both assume a priori FCC packing of spheres and proceed to calculate micelle core size and intermicelle distance as a function of block molecular weight and composition. Leibler's[5] approach utilizes fluctuation theory to determine the symmetry of the microphase separated state at the onset of the transition from the high-temperature homogeneous state. He evaluated several possible lattice types for spherical domains (SC, BCC, FCC, and rhombohedral) and found that the BCC arrangement offered the lowest free energy. Ohta and Kawasaki's recent calculations show that a BCC arrangement is only slightly more favored than FCC[6].

The best experimental evidence[7,8] for the lattice type of block copolymer samples exhibiting a spherical microdomain morphology strongly suggests a BCC arrangement does indeed occur, although there are a number of published reports of SC, FCC, and even orthorhombic arrangements.[9-13] The data are of two kinds: (i) TEM of $OsO_4$-stained sections wherein different symmetry projections are identified and assigned to various (*hkl*) projections and the relative interdomain spacings compared to the various lattice arrangements and (ii) SAXS of bulk samples where based on micelle core size from the position of the form factor peak and on the intermicelle separation from the position of the lower angle interference peaks, the volume fraction of domains is compared to the known volume fraction of the domain forming minority component. A critical issue on proper assignment of the lattice type is attainment of pseudoequilibrium conditions—evidenced by development of long-range order in the sample. In all cases the studies[9-13] suggesting non-BCC structures suffer from the lack of well-developed long-range order, and, for this reason, their assignment of a particular lattice type is highly suspect.

In the course of our investigations on diblock copolymers, we have encountered the ordering of spherical domains in bulk and in ultrathin films. As will be shown, the lattice structure of spherical microdomains in the bulk

† Present address: 3M Center, Building 236-38-01, St. Paul, MN 55125.
‡ Present address: Monsanto Company, 730 Worcester Street, Springfield, MA 01151.

0024-9297/87/2220-2934$01.50/0 

Table I
Molecular Characteristics of Block Copolymers

| sample | $M_n$ STY, kg/mol | wt % STY | $M_n$ BUT, kg/mol | $M_w/M_n$[d] | vol % STY |
|---|---|---|---|---|---|
| SB1 | 10.5[a] | 8.48[b] | 113[c] | 1.06 | 7.43 |
| SB2 | 56.6[e] | 83.9[b] | 10.9[d] | 1.04 | 81.8 |

[a] Information provided by Shell. [b] Determined from UV analysis. [c] Calculated from *a* and *b*. [d] Obtained from GPC. [e] Calculated from *b* and *d*.

is indeed BCC; however, in thin films consisting of only a monolayer of domains, the packing is hexagonal (HEX). An extremely simple suggestion of Sir Charles Frank[14] to consider the optimum covering fraction lattice provides an explanation of why the bulk lattice type is BCC and also explains the transition in lattice from BCC to HEX for ultrathin films.

## Experimental Section

**Sample Synthesis.** Two different styrene–butadiene (SB) diblock copolymers, designated SB1 and SB2, were studied. Their molecular characteristics are given in Table I. Sample SB1 was an experimental polymer provided by Dr. D. L. Handlin, Jr., of Shell Development Co., while sample SB2 was synthesized by Dr. L. J. Fetters of Exxon Research and Engineering Co. Synthesis was performed via the usual anionic technique employed for styrene–diene block copolymers.[15] Purified butadiene (or styrene) monomer, benzene solvent, and *sec*-butyllithium initiator are allowed to react completely at 30 °C under high vacuum, after which a small sample is removed from the reaction flask for later analysis. The second monomer is then added to the reactor and allowed to react. The reaction is subsequently terminated by addition of degassed methanol.

**Molecular Characterization.** The molecular weight distributions of the block copolymers and the samples removed from the reactor after polymerization of the first block were obtained with a Waters 150C gel permeation chromatograph which had been calibrated with several polystyrene standards. In addition, the block copolymer compositions were determined by UV absorption in tetrahydrofuran at a wavelength of 260 nm. The molecular weights of the majority component blocks were then calculated from the minority component block molecular weight obtained from GPC and the composition determined by UV analysis. The characterization is presented in Table I. Although the microstructure of the polybutadiene was not determined, typical microstructures obtained from such anionic polymerizations contain approximately 90% mixed 1,4 cis and trans and 10% 1,2 addition.

**Structural Characterization.** Thick films for SAXS and EM were prepared by solvent casting from a 5% w/v solution of the block copolymer in toluene, a nonpreferential solvent. A volume of solution needed to prepare a 1-mm thick film was placed in a loosely covered glass casting dish at 50 °C, and the solvent was allowed to evaporate over a period of approximately 1 week. The sample was then placed under vacuum to assure complete removal of the solvent. Subsequently, the film was placed in a glass tube connected to a high vacuum line ($\sim 10^{-5}$/torr). After being pumped for 12 h, the tube was sealed off from the vacuum line with a torch. The sealed tube was then placed in a vacuum oven for 2 weeks at 120 °C to further order the sample. This procedure was necessary to prevent degradation, i.e., oxidative cross-linking, of the unsaturated polybutadiene during annealing. The sample preparation method used was designed to provide a bulk sample with an equilibrium morphology, typified by a high degree of long-range order. Thin sections approximately 500 Å thick for TEM were obtained by cryoultramicrotomy at −110 °C with a diamond knife on an AO Reichert Ultracut microtome with an FC4 cryo attachment. The thin sections were stained by exposing them to $OsO_4$ vapors for 4 h.

Ultrathin films in which to study the two-dimensional order of domains were also cast from a toluene solution. For these films, a very dilute solution ($\sim$0.05 w/v %) of the copolymer SB2 in toluene was made. Drops of this solution were then placed on a carbon-coated glass slide. Upon evaporation of the toluene, extremely thin film "droplets" of the copolymer are left on the slide. These specimens were then annealed under vacuum at 120 °C for several hours; this procedure ensures that any residual solvent is removed from the polymer and that the sample is allowed to attain its equilibrium morphology. After annealing, the carbon coating was separated from the glass slide by immersing the slide into a distilled water bath. The carbon layer (which acts as a substrate for the polymer films) floats on the water bath allowing the polymer film and its carbon support to be picked up on the top of TEM grids. The samples were then stained in $OsO_4$ vapor.

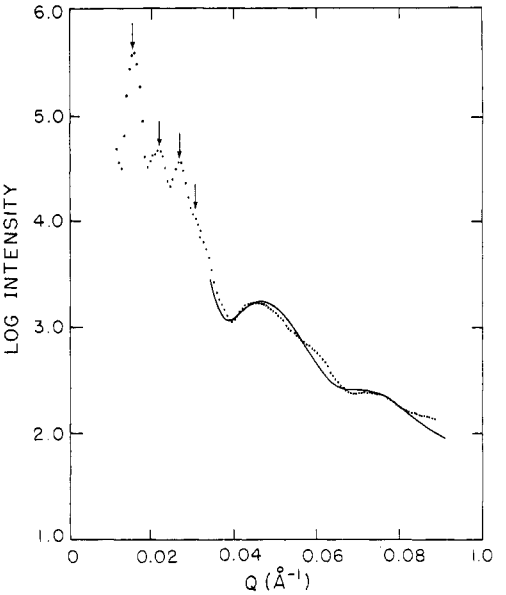


**Figure 1.** Corrected SAXS data for sample SB1. The solid line shows the sphere scattering fit to the data taking into account the distribution in sphere size and diffuse domain boundary.

A JEOL 100CX electron microscope operated at 100 KV was used to examine both the sections prepared from the bulk specimens as well as the ultrathin solution cast sample. A side entry gonimeter and tilt-rotate specimen holder allowed the sections to be rotated ±180° in the plane of the specimen and tilted about any chosen axis by ±60°.

Small-angle X-ray scattering was performed with a 1-kW nickel-filtered copper source and Kratky collimation with a 40-μm entrance slit and 50-cm flight path. The scattering data were recorded by using a Braun one-dimensional position sensitive detector and were corrected for sample absorption, detector wire sensitivity, parasitic scattering, and slit length smearing. Desmearing was performed by using Vonk's FFSAXS version 3 program.[16]

## Results and Discussion

**Bulk Lattice: BCC.** The corrected SAXS curve for sample SB1 is shown in Figure 1. The scattered intensity is plotted as the log of the number of X-ray counts recorded at a particular scattering vector **Q** ($4\pi(\sin\theta)/\lambda$). Sample SB1 exhibits three well-defined low angle interference peaks associated with the lattice of spherical microdomains. In addition, there are weaker, broad peaks at higher angle attributable to intraparticle sphere scattering. The $Q$ values of the lattice peaks are 0.0160, 0.0226, and 0.0273 Å$^{-1}$. Comparing the relative spacings of the reflections with those of various possible lattices reveals excellent agreement for either a SC or BCC lattice (these two lattices have the same $d$-spacing ratios until the seventh-order reflection). When the micelle core size is calculated from the form factor peak position ($Q \approx 0.05$ Å$^{-1}$) and the first interference peak is assigned as either (100) for SC or (110) for BCC, the volume fraction of spherical domains may be determined. The average sphere radius is approximately 116 Å, and the average lattice parameters

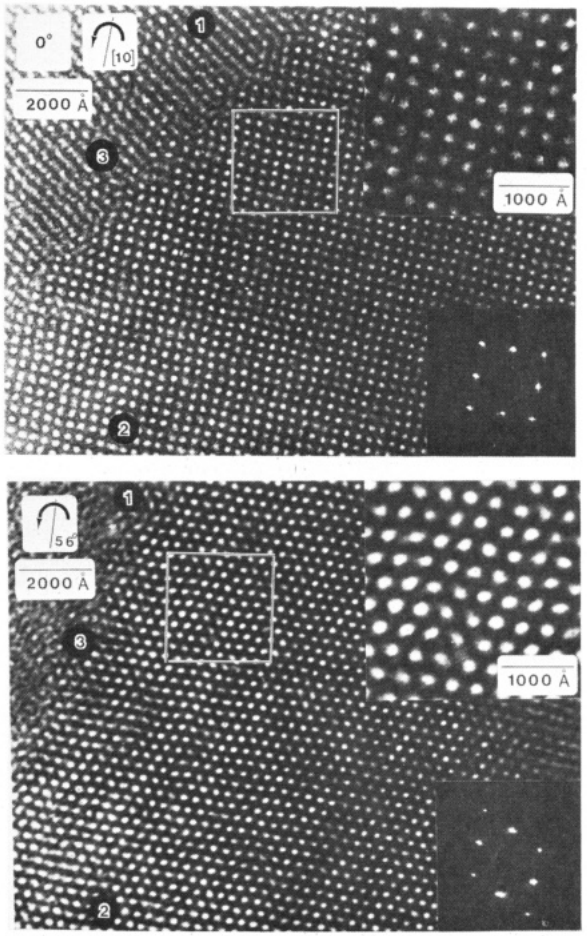


**Figure 2.** Electron micrographs showing the (a) (100) and (b) (111) projections of the BCC macrolattice for SB1. The dark circular regions labeled 1, 2, and 3 are polystyrene spheres deposited on the section to confirm the axis and magnitude of tilt between the two projections. Optical diffraction patterns are given in the bottom right inset of each figure.

are 397 Å for SC and 563 Å for BCC. The volume fraction assuming a SC arrangement of polystyrene spherical micelles is therefore 0.105 and that assuming a BCC arrangement 0.073. The actual volume fraction of polystyrene is 0.0743 assuming densities of 1.05 and 0.91 g/cm$^3$ for polystyrene and polybutadiene, respectively. Thus as previously found by Bates et al.,[8] a BCC arrangement is decisively favored.

Bright field TEM of $OsO_4$-stained microtome sections confirms the BCC arrangement. Figure 2a shows a fourfold symmetric projection of sample SB1; as expected the minor component polystyrene constitutes the spherical domains. When tilt experiments are performed in the TEM utilizing the goniometer stage, a systematic series of two-dimensional projections can be obtained from a given area from which the three-dimensional structure can be conclusively determined. The (100), (110), and (111) projections for the SC, BCC, and FCC lattices are displayed in Figure 3. In each case the unit cell has been outlined and the projected distances between neighboring spheres indicated. It is possible to straightforwardly distinguish between the SC and BCC packing modes using the tilt method shown schematically in Figure 4. An area (single grain) in the correct orientation to give a square projection [i.e. the (100) projection] is first located. This region is then tilted about either the axis designated [10] or [11] in Figure 4. Tilting about the [10] axis is equivalent to tilting about the [100] SC axis or the [110] BCC axis. Similarly, tilting about the [11] axis is equivalent to tilting about the [110] SC axis

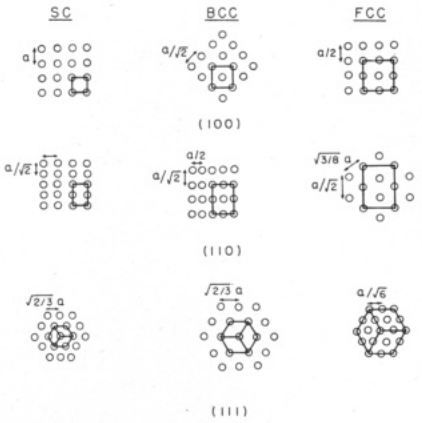


**Figure 3.** (100), (110), and (111) projections of a SC, BCC, and FCC lattice showing the unit cells (outlined) and relative projected intersphere distances (adapted from Skoulios[20]). The square arrays of the (100) projections have been drawn the same size leading to different unit cell sizes for the three lattice types. Subsequent projections have been scaled accordingly.

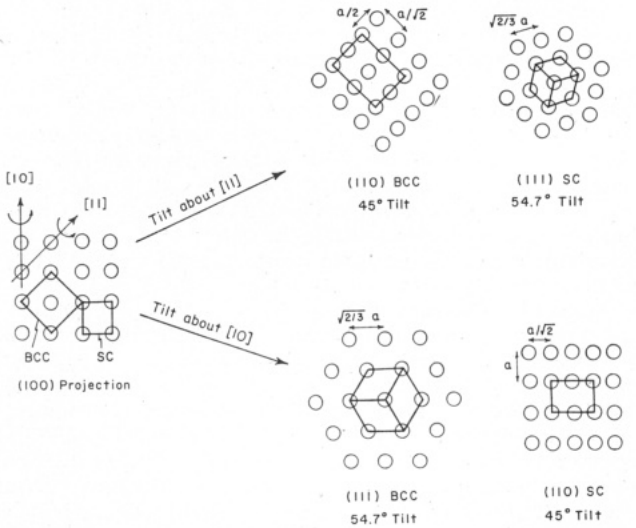


**Figure 4.** Schematic of tilting experiment performed in the electron microscope relevant to Figure 2a,b.

or the [100] BCC axis. Therefore, as shown in Figure 4, tilting about the [10] or [11] axis will produce different projections depending on lattice type. Figure 2a,b shows the effect of tilt of a square projection about the [10] axis. The amount of tilt to produce the sixfold symmetric projection was 56° according to the goniometer. This is confirmed by triangulating between the positions of the three landmark polystyrene latex spheres previously deposited on the upper surface of the section in the two images. The tilt angle expected for the BCC structure is 54.7° in excellent agreement with the experimental value and unequivocally proving a BCC arrangement.

**Thin Film Lattice: HEX.** A bright field TEM image of an $OsO_4$-stained solution cast film of the SB2 sample is shown in Figure 5. The sample is about one domain thick and displays a sixfold symmetric packing arrangement of polybutadiene micelles. Tilting the sample confirms that the domains are spherical and the sample consists of only one layer. The hexagonal lattice spacing is approximately 375 Å with an average domain radius of 90 Å.

**Lattice Type for Spherical Microdomains.** Since the composition of both block copolymer samples is such that the minority phase is less than about 20% by volume, each system chooses to adopt a spherical microdomain morphology. At equilibrium, the preferred packing arrange-

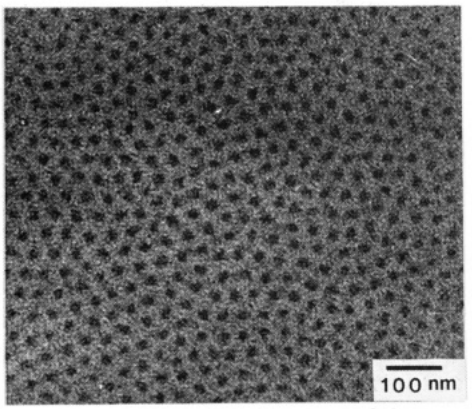


**Figure 5.** Electron micrograph of ultrathin film of sample SB2 displaying hexagonal packing of the spherical microdomains.

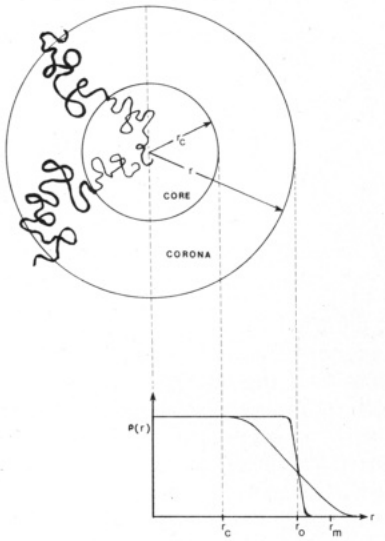


**Figure 6.** (a) Schematic of spherical diblock copolymer micelle indicating core and corona regions. (b) Segmental density distributions.

ment of the spherical microdomains will be that which corresponds to the lowest free energy. A simple approach suggested to us by Sir Charles Frank[14] is to consider the covering of all space by the spherical micelles. We develop his idea as follows: when the block copolymer undergoes phase separation, aggregates of chains form spherical micelles. These micelles then interact during the evaporation of solvent to form an ordered array. We assume that the micelle volume remains a constant after solvent removal. We denote the micelle center region containing the minority component as the core (of radius $r_c$) which is surrounded by a concentric corona region of the majority component outer chains (see Figure 6a). The corona region will be considered a penetrable shell due to the falloff, with increasing radial distance, of segmental density of the outer chains (see Figure 6b). To uniformly fill the matrix, chains from neighboring coronae must overlap and interpenetrate to fully cover all of the matrix space of uniform density. Clearly the particular choice of lattice arrangement of the micelles principally affects the material in the outermost regions of the coronae. The problem thus becomes one of examining various lattice arrangements toward their influence on the outerblock chain conformations.

We construct our model lattices such that the nearest neighbor lattice points are separated by a distance $2R$. In 2D the *covering fraction* for a given lattice is defined as the area covered by penetrable (i.e. "soft") circles per unit area of the plane. The more familiar *packing fraction* is the area covered by circles when they just touch ("hard" circles, $r = R$). Referring to Figure 7, the covering fraction $A_C$ for the square lattice of overlapping circles $r \geq R$ is given by

$$A_C^{SQ} = \tfrac{1}{2}(r/R)^2[(\pi/2) - \theta + \sin\theta] \quad (1)$$

with

$$\theta = 2\cos^{-1}(R/r) \quad (2)$$

The circles begin to overlap for $r > R$ with the overlap area fraction given by

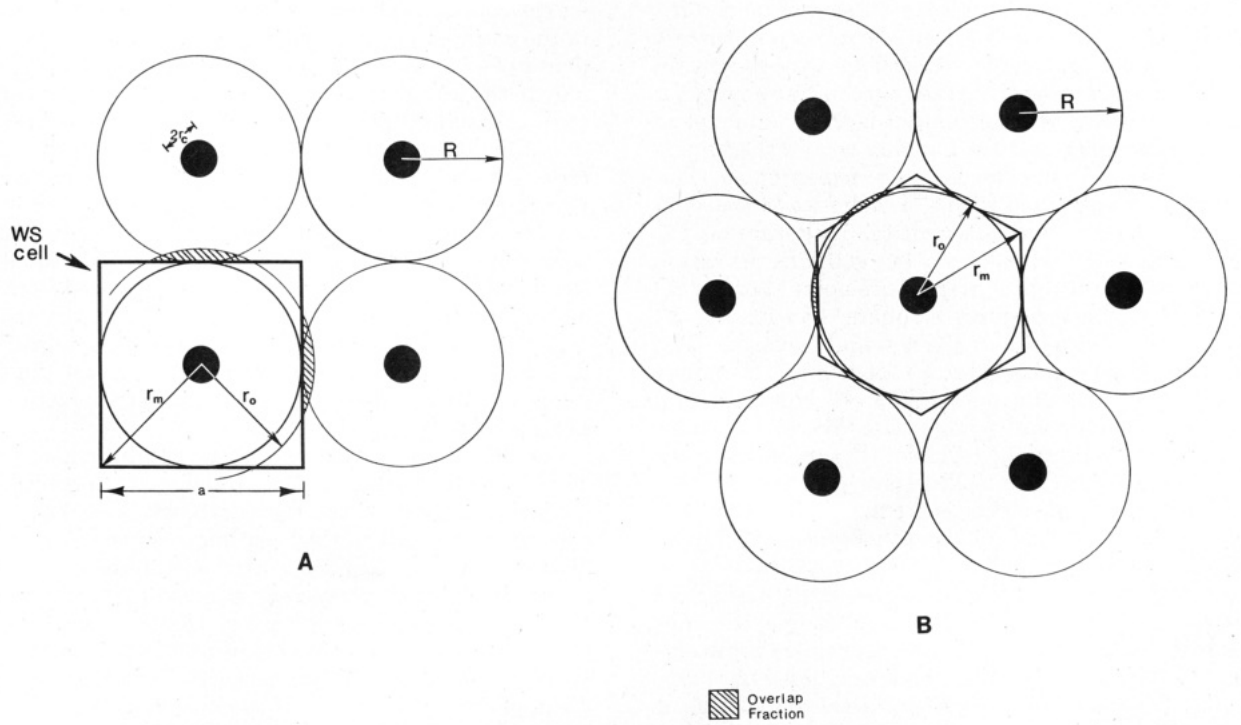


**Figure 7.** Covering of the plane by (a) square lattice and (b) hexagonal lattice. The shaded region represents the overlap material that must be redistributed to the interstitial regions to uniformly cover the plane.

$$A_O^{SQ} = (4/\pi)[\theta - \sin\theta] \quad (3)$$

The hexagonal covering fraction is given by

$$A_C^{HEX} = \frac{\sqrt{3}}{6}\left(\frac{r}{R}\right)^2[\pi - 3\theta + 3\sin\theta] \quad (4)$$

and the overlap fraction is given by

$$A_O^{HEX} = (6/\pi)[\theta - \sin\theta] \quad (5)$$

In 3D the covering fraction $V_C$ is defined as the volume occupied by penetrable spheres per unit volume. The covering fractions for the SC, BCC, and FCC lattices of overlapping spheres ($r > R$) are given by[17]

$$V_C^{SC} = \frac{\pi}{12}\left(\frac{r}{R}\right)^3\left[-4 + 9\left(\frac{R}{r}\right) - 3\left(\frac{R}{r}\right)^3\right] \quad R < r < \sqrt{2}R \quad (6)$$

$$V_C^{BCC} = \frac{\sqrt{3}\pi}{8}\left(\frac{r}{R}\right)^3\left[-3 + 6\left(\frac{R}{r}\right) - 2\left(\frac{R}{r}\right)^3\right] \quad R < r < \frac{2}{\sqrt{3}}R \quad (7)$$

$$V_C^{FCC} = \frac{\pi}{\sqrt{2}}\left(\frac{r}{R}\right)^3\left[-\frac{5}{3} + 3\left(\frac{R}{r}\right) - \left(\frac{R}{r}\right)^3\right] \quad R < r < \frac{2}{\sqrt{3}}R \quad (8)$$

Their overlap fractions $V_O$ are given by

$$V_O^i = C_i[2 - 3(R/r) + (R/r)^3] \quad (9)$$

where $C_i = 3$ for SC, 4 for BCC, and 6 for FCC.

In the actual situation of the ordering of block copolymer micelles, instead of a fixed-size lattice with expanding circles (spheres), the micelle core size is approximately constant while the lattice contracts. As the micelles approach one another, the overlap regions along the lines connecting core centers build an excess of segmental density. The remaining interstitial regions have, however, a density deficiency so that the outer block chains in the corona must deform to redistribute the segmental density. Thus the intermicelle distance will decrease until there is sufficient overlap material to redistribute to uniformly fill the interstitial volume. The difference in free energy for the various lattices will depend on both the amount of material overlapped and the distance to and the type of region over which this material must be redistributed. This can be readily visualized with the reference to the Wigner–Seitz cell of the particular lattice. By definition, the Wigner–Seitz (WS) cell of the lattice contains the region of lattice space closest to a given lattice point. For the 2D square lattice the WS cell is a square, and for the 2D hexagonal lattice the WS cell is a simple hexagon. The hard circle (sphere) contact radius (denoted $R$) is equivalent to the closest point on the WS cell boundary to a lattice point; the furthest point on the WS cell boundary corresponds to the furthest region of the interstitial space (a distance $r_m$ from the micelle center). In the 3D case, the WS cell of the SC lattice is a cube, that of the BCC lattice a truncated octahedron, and that of the FCC lattice a rhombic dodecahedron.[18]

We consider the two-dimensional case first. The actual situation even in an ultrathin film is, of course, three-dimensional, but the covering fraction problem is two-dimensional for a monolayer of domains (it is, in fact, approximately equivalent to the three-dimensional case of cylindrical domain packing). We assume that the film has a uniform thickness, $t$, and that the domain cores are centered at $t/2$.[19] The corona regions of the micelles must overlap and deform to provide uniform filling of the matrix space and planar film surfaces.[16]

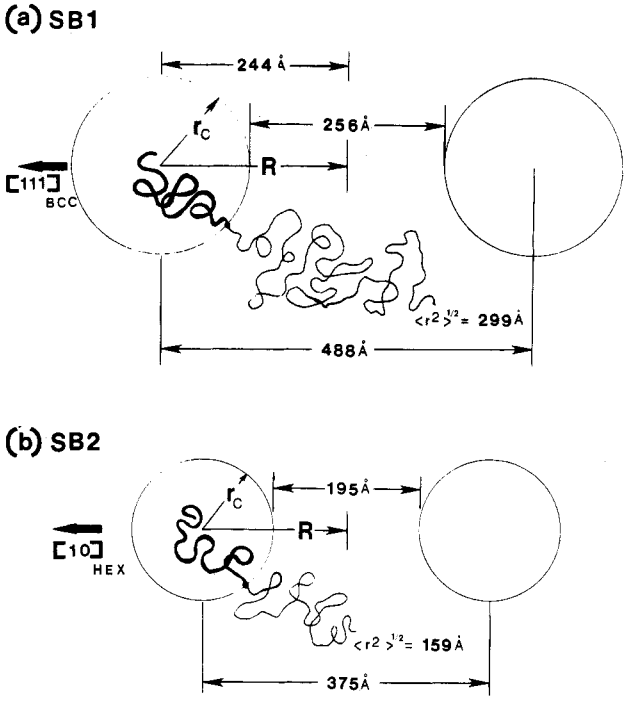


**Figure 8.** Schematic of core and corona regions of adjacent micelles for samples SB1 and SB2.

We propose that the lattice packing arrangement will be that which requires the least redistribution of material from regions of excess segmental density. The extent of segmental redistribution to provide a uniform density throughout the matrix phase will depend on the amount and location of the material in the overlap fraction relative to the remaining interstitial regions in the partial covered space. The overlap fraction depends on the lattice type and the extent of overlap, i.e. the value of $r$ relative to $R$. In order to compare the overlap fraction for each lattice we consider two extremes for the segmental density profile of the corona chains (recall Figure 6b). If the segmental density falloff is sharp, the micelles need to interpenetrate only to the extent that the covering fraction plus $^1/_2$ of the overlap fraction totals unity (i.e., the volume of the WS cell of the lattice is set equal to the micelle volume). The radius of the micelle for this situation is denoted $r_0$ (see Figure 7). The other possibility is to consider that the segmental density profile falls off gradually, necessitating significant overlap of neighboring coronae. Fortunately, the degree of interpenetration can be estimated from the measured structural data. Figure 8 depicts the spatial arrangements along the [111] nearest-neighbor direction in the BCC lattice for sample SB1 and along the [10] nearest-neighbor direction in the 2D HEX lattice for sample SB2.

For SB1 the molecular weight of the butadiene block comprising the corona is 113 000, and for sample SB2, the molecular weight of the styrene block is 56 600. The corresponding unperturbed root-mean-square end-to-end distances, $\langle r^2\rangle^{1/2}$, are 299 and 159 Å, respectively. Of course, in the microphase-separated state, the chains will not obey Gaussian statistics but these parameters are useful to compare to those of the assumed model: $r_c$, $R$, $r_0$, and $r_m$. For the BCC lattice of sample SB1, the shortest distance from the surface of the micelle core to the WS cell boundary, $R - r_c$, is only about 130 Å, while the greatest distance from the surface of the micelle core to the WS

**Table II**
**Overlap Parameters for Various Lattice Types**

2-D

| lattice | $r_0$[a] | $A_0$ ($r_0$) | $r_m$[b] | $A_0$ ($r_m$) |
|---|---|---|---|---|
| SC | 1.128$R$ | 0.18 | 1.414$R$ | 0.73 |
| HEX | 1.05$R$ | 0.074 | 1.155$R$ | 0.09 |

3-D

| lattice | $r_0$[c] | $V_0$ ($r_0$) | $r_m$[d] |
|---|---|---|---|
| SC | 1.241$R$ | 0.317 | 1.732$R$ |
| BCC | 1.137$R$ | 0.167 | 1.291$R$ |
| FCC | 1.105$R$ | 0.157 | 1.414$R$ |

[a] $r = r_0$ when $A_C + {}^1/_2A_0 = 1.0$. [b] $r = r_m$ when $A_C = 1.0$. [c] $r = r_0$ when $V_C + {}^1/_2V_0 = 1.0$. [d] $r = r_m$ when $V_C = 1.0$.

cell boundary, $r_m - r_c$, is about 200 Å. Both distances are significantly smaller than $\langle r^2\rangle^{1/2}_{PB}$, indicating that corona chains from neighboring micelles strongly overlap. For the HEX lattice of sample SB2, the distances $R - r_c$ and $r_m - r_c$ are approximately 100 and 130 Å, again considerably less than the $\langle r^2\rangle^{1/2}_{PS}$, suggesting substantial interpenetration of coronae. These structural distance data thus imply the actual micellar segmental density profile falloff is gradual and suggest the evaluation of the various lattice arrangements should be based on a micelle radius larger than $r_0$. From our model, we assume this situation corresponds to a micelle radius equal to the furthest distance on the WS cell boundary, $r_m$.

In 2D the hexagonal lattice provides the best mode of packing based on calculations assuming either a micelle radius of $r_0$ or $r_m$ (see Table II). For the case of a sharp segmental density profile, the micelle radius, $r_0$, is 1.128$R$ for the SC lattice but only 1.050$R$ for the HEX lattice, with corresponding overlap fractions of 0.18 for SC and 0.074 for HEX. For the case of a gradual falloff in segmental density, the micelle radius, $r_m$, is 1.414$R$ for the SC lattice but only 1.155$R$ for the HEX lattice with corresponding overlap fractions of 0.73 and 0.09, respectively. Thus despite the 1.5$X$ higher overlap fraction for the HEX lattice relative to the SC lattice for a given value of $r/R$, the inherenty better covering by the hexagonal arrangement provides the lowest overlap fraction with least required redistribution of material from regions of excess segmental density.

In 3D, one expects the most efficient packing scheme, namely, FCC packing, to provide the optimum covering lattice. Indeed for the sharp segmental density falloff situation ($r = r_0$), the overlap fractions have values of 0.317, 0.167, and 0.157 for the SC, BCC, and FCC lattices, respectively. The SC arrangement is very disfavored, but the FCC lattice has only a slightly lower overlap fraction than a BCC arrangement of micelles. Furthermore, because of its larger $r_m$ value (1.414$R$ vs. 1.291$R$), the energy cost for redistribution of the overlapped material will be higher for the FCC lattice relative to the BCC lattice, suggesting that the FCC and BCC lattices may be nearly equivalently good for micelle packing in this situation. For the case of a gradual falloff in segmental density, the overlap fractions should be compared for $r = r_m$. This calculation is unfortunately extremely difficult because for $r > 1.155R$, overlapping of already overlapped regions begins as well as overlapping of second nearest neighbors. Quantitatively it is straightforward to note that at a given value of $r/R$, the overlap fraction will be considerably larger for the FCC lattice compared to the BCC lattice, due to the higher coordination number of each sphere. The deciding factor, unlike the 2D case, is the larger (not smaller) value of $r_m$ for the most efficient packing lattice. In other words, considering a 3D lattice arrangement of penetrable spheres, the matrix is fully covered (i.e. the sphere radius reaches $r_m$ of the WS cell) with the smallest value of $r$ and the lowest overlap fraction for BCC packing.

## Conclusions

Upon phase separation block copolymer chains can aggregate to form spherical microdomains. It is proposed that the ordered arrangement of these micelles is determined by the optimum covering lattice that minimizes the unfavorable conformations necessitated by the deformation of the interpenetrating corona chains to uniformly fill the matrix space. For thin films containing only a single layer of spherical micelles, the optimum covering lattice is hexagonal. For bulk, three-dimensional samples, the optimum covering lattice is body centered cubic.

**Acknowledgment.** Financial support from the National Science Foundation, Grant DMR 84-06079 (Polymers Division), and from Union Carbide Corp. (DJK Fellowship) and Monsanto Co. (DBA Fellowship) is gratefully acknowledged. We also thank Dr. L. J. Fetters of Exxon Research and Engineering Co. and Dr. D. L. Handlin, Jr., of the Shell Development Co. for providing samples and the NSF Materials Research Laboratory at the University of Massachusetts for facilities. E.L.T. thanks Sir Charles Frank for stimulating discussions.

**Registry No.** SB (block copolymer), 106107-54-4.

## References and Notes

(1) Molau, G. E. *Block Copolymers*; Aggarwal, S. L., Ed.; Plenum: New York 1970.
(2) Thomas, E. L.; Alward, D. B.; Kinning, D. J.; Martin, D. C.; Handlin, D. L., Jr.; Fetters, L. J. *Macromolecules* **1986**, *19*, 2197.
(3) Meier, D. J. *Block and Graft Copolymers*; Burke, J. J., Weiss, V., Eds.; Syracuse University Press: Syracuse, NY, 1973.
(4) Helfand, E.; Wasserman, Z. R. *Developments in Block Copolymers–I*; Goodman, I., Ed.; Applied Science Publishers: New York, 1982.
(5) Leibler, L. *Macromolecules* **1980**, *13*, 1602.
(6) Ohta, T.; Kawasaki, K. *Macromolecules* **1986**, *19*, 2621.
(7) Pedemonte, E.; Turturro, A.; Bianchi, V.; Devetta, P. *Polymer* **1973**, *14*, 145.
(8) Bates, F. S.; Cohen, R. E.; Berney, C. V. *Macromolecules* **1982**, *15*, 589.
(9) Hashimoto, T.; Fujiura, M.; Kawai, H. *Macromolecules* **1980**, *13*, 1660.
(10) Roe, R. J.; Fishkis, M.; Chang, V. C. *Macromolecules* **1981**, *14*, 1091.
(11) Richards, R. W.; Thomason, J. L. *Polymer* **1981**, *22*, 581.
(12) Richards, R. W.; Thomason, J. L. *Macromolecules* **1983**, *16*, 982.
(13) Gallot, B. R. M. *Adv. Polym. Sci.* **1979**, *29*, 85.
(14) Frank, Sir Charles, private communication to ELT, April, 1985.
(15) Fetters, L. J. *J. Polym. Sci.* C **1969**, *26*, 1.
(16) Vonk, C. G. *J. Appl. Crystallogr.* **1971**, *4*, 340.
(17) HCP, which is also a close packed structure, gives the same results as FCC for $R < r < (2/(3)^{1/2})R$.
(18) In their paper on spherical microdomains, Helfand and Wasserman [*Macromolecules* **1978**, *11*, 960] approximated the WS cell of the assumed FCC lattice as a sphere of equivalent volume so as to be able to separate the differential equations governing domain size and separation distance.
(19) Accommodation by variation in local film thickness is also possible. Metal shadowing indicates, however, the upper film surface is nearly planar.
(20) Skoulios, A. E. *Developments in Block Copolymers-2*; Goodman, I., Ed.; Applied Science Publishers: New York, 1982.